J|A|C|S ARTICLES

Published on Web 03/10/2010

New Light on NO Bonding in Fe(III) Heme Proteins from Resonance Raman Spectroscopy and DFT Modeling

Alexandra V. Soldatova,[†] Mohammed Ibrahim,[†] John S. Olson,*[,‡] Roman S. Czernuszewicz,*[,§] and Thomas G. Spiro*[,†]

Department of Chemistry, University of Washington, Box 351700, Seattle, Washington 98195, Department of Biochemistry and Cell Biology, Rice University, Houston, Texas 77005, and Department of Chemistry, University of Houston, Houston, Texas 77204

Received July 24, 2009; E-mail: spiro@chem.washington.edu; roman@uh.edu; olson@rice.edu

Abstract: Visible and ultraviolet resonance Raman (RR) spectra are reported for $Fe^{III}(NO)$ adducts of myoglobin variants with altered polarity in the distal heme pockets. The stretching frequencies of the $Fe^{III}-NO$ and N−O bonds, ν_{FeN} and ν_{NO}, are negatively correlated, consistent with backbonding. However, the correlation shifts to lower ν_{NO} for variants lacking a distal histidine. DFT modeling reproduces the shifted correlations and shows the shift to be associated with the loss of a lone-pair donor interaction from the distal histidine that selectively strengthens the N−O bond. However, when the model contains strongly electron-withdrawing substituents at the heme β-positions, ν_{FeN} and ν_{NO} become positively correlated. This effect results from $Fe^{III}-N-O$ bending, which is induced by lone-pair donation to the N_{NO} atom. Other mechanisms for bending are discussed, which likewise lead to a positive ν_{FeN}/ν_{NO} correlation, including thiolate ligation in heme proteins and electron-donating *meso*-substituents in heme models. The ν_{FeN}/ν_{NO} data for the Fe(III) complexes are reporters of heme pocket polarity and the accessibility of lone pair, Lewis base donors. Implications for biologically important processes, including NO binding, reductive nitrosylation, and NO reduction, are discussed.

Introduction

Heme protein sensors[1−3] of the gaseous ligands CO, NO, and O_2 play key regulatory roles in biology. Other heme proteins catalyze oxidative or reductive chemistry of the same ligands. The nature of the heme−ligand adducts and their interactions with the surrounding protein are of continuing interest.

Among these ligands, NO is unique in being able to bind heme in both Fe(II) and Fe(III) oxidation states. The odd electron on NO gives it flexible electronic properties. $Fe^{III}(NO)$ adducts are often transient, being easily reduced to the more stable $Fe^{II}(NO)$ adducts. However, $Fe^{III}(NO)$ is stabilized in some heme proteins. These include the nitrophorins,[4] used by blood-sucking insects to release NO as a vasodilator into the victim's bloodstream. Maintaining the Fe(III) oxidation state assures reversible binding and release of NO. $Fe^{III}(NO)$ is also involved in the catalytic cycle of NO synthases[5] and of NO redox enzymes, including nitrite reductase[6] and NO reductase.[7]

The dominant mechanism for XO binding to heme (X = C, N, O) is backbonding, because the ligands have low-lying π^* orbitals, well matched to the filled d_π orbitals on Fe(II). These orbitals are contracted in Fe(III), which is unable to bind CO or O_2. However, the odd electron on NO can readily transfer to Fe(III), producing the $Fe^{II}(NO^+)$ resonance structure, isoelectronic with $Fe^{II}(CO)$. DFT computations on the model heme adduct show that $Fe^{II}(NO^+)$ is indeed the appropriate description of the $Fe^{III}(NO)$ ground state.[8] However, Lehnert and co-workers report computation of a low-energy $Fe^{III}(NO)$ radical state, in which the $Fe^{III}-NO$ bond is slightly elongated and the odd electrons on Fe(III) and NO are antiferromagnetically coupled.[8] This state is likely involved in the mechanism of $Fe^{III}-NO$ dissociation. Walker discussed this state previously and pointed out that it should be stabilized by porphyrin ruffling, a structural feature of the nitrophorins.[4]

Backbonding produces an anticorrelation of the Fe−XO and X−O bond strengths, in response to polarization effects. Enhancement of backbonding strengthens Fe−XO while weakening X−O. Negative correlations between Fe−XO and X−O stretching frequencies, gathered from Raman and/or IR spectra,

[†] University of Washington.
[‡] Rice University.
[§] University of Houston.

(1) Chan, M. K. *Curr. Opin. Chem. Biol.* **2001**, *5*, 216–222.
(2) Gilles-Gonzalez, M.-A.; Gonzalez, G. *J. Inorg. Biochem.* **2005**, *99*, 1–22.
(3) Aono, S. *Dalton Trans.* **2008**, 3137–3146.
(4) Walker, F. A. *J. Inorg. Biochem.* **2005**, *99*, 216–236.
(5) Rousseau, D. L.; Li, D.; Couture, M.; Yeh, S. R. *J. Inorg. Biochem.* **2005**, *99*, 306–323.
(6) George, S. J.; Allen, J. W. A.; Ferguson, S. J.; Thorneley, R. N. F. *J. Biol. Chem.* **2000**, *275*, 33231–33237.
(7) Pinakoulaki, E.; Gemeinhardt, S.; Saraste, M.; Varotsis, C. *J. Biol. Chem.* **2002**, *277*, 23407–23413.
(8) Praneeth, V. K. K.; Paulat, F.; Berto, T. C.; DeBeer George, S.; Nather, C.; Sulok, C.; Lehnert, N. *J. Am. Chem. Soc.* **2008**, *130*, 15288–15303.
(9) Spiro, T. G.; Ibrahim, M.; Wasbotten, I. H. In *The Smallest Biomolecules*; Ghosh, A., Ed.; Elsevier: New York, 2008; pp 96−123.
(10) Linder, D. P.; Rodgers, K. R. *Inorg. Chem.* **2005**, *44*, 1367–1380.
(11) Linder, D. P.; Rodgers, K. R.; Banister, J.; Wyllie, G. R. A.; Ellison, M. K.; Scheidt, W. R. *J. Am. Chem. Soc.* **2004**, *126*, 14136–14148.
(12) Vogel, K. M.; Kozlowski, P. M.; Zgierski, M. Z.; Spiro, T. G. *Inorg. Chim. Acta* **2000**, *297*, 11–17.
(13) Vogel, K. M.; Kozlowski, P. M.; Zgierski, M. Z.; Spiro, T. G. *J. Am. Chem. Soc.* **1999**, *121*, 9915–9921.

 10.1021/ja906233m

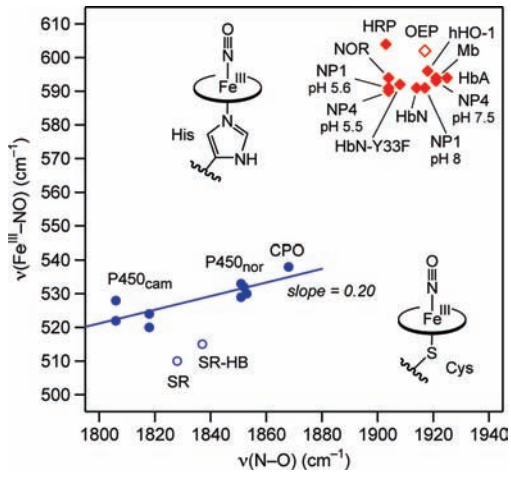

Figure 1. ν_{FeN}/ν_{NO} data for six-coordinate $Fe^{III}(NO)$ heme proteins and model complexes (see Table 1). "◆" indicates histidine-ligated heme-protein adducts, while "●" indicates cysteine-ligated heme-protein adducts; "◇" and "○" represent $Fe^{III}(NO)$ porphyrin model complexes. The blue line is a linear correlation for thiolate-ligated adducts, with $r = 0.84$, after excluding the data for model complexes (SR and SR-HB).

have been observed for Fe(II) adducts of all three XO ligands.[9] However, $Fe^{III}(NO)$ adducts are exceptional. When the available literature data are plotted (Figure 1), the dominant ν_{FeN}/ν_{NO} correlation seems to be *positive*; the $Fe^{III}-NO$ and N−O bond strengths increase or decrease in concert for oxidized iron. Rodgers and co-workers[10,11] have investigated this phenomenon computationally and have found *positive* ν_{FeN}/ν_{NO} correlations when electron-donating and -withdrawing heme *meso*-substituents were used to polarize the $Fe^{III}(NO)$ adduct, a technique used previously,[12,13] both experimentally and computationally to explore the *negative* correlations found for $Fe^{II}(XO)$ adducts. They attributed the contrary behavior of $Fe^{III}(NO)$ to a unique occupied molecular orbital that is antibonding with respect to both the $Fe^{III}-NO$ and N−O bonds.[10,11]

However, the available experimental data are sparse (Table 1), owing to the limited stability of $Fe^{III}(NO)$ adducts. The data describing the positive correlation in Figure 1 are all from thiolate-ligated heme proteins and models. The available data for non-thiolate adducts appear as a scattered cluster in the upper right corner of the figure. To examine this cluster more closely, we have obtained a new data set from resonance Raman (RR) spectra of a series of myoglobin (Mb) variants, used previously to explore backbonding in $Fe^{II}(CO)$[14] and $Fe^{II}(NO)$[15] complexes (Figure 2). These data reveal *negative* ν_{FeN}/ν_{NO} correlations for $Fe^{III}(NO)$ adducts, fully consistent with backbonding. They also reveal a specific N−O strengthening effect that is associated with the distal histidine of Mb. DFT modeling confirmed the latter effect, showing it to result from a lone-pair interaction of the imidazole with the positively charged $Fe^{II}(NO^+)$, an effect that was originally postulated by Miller et al.[16] Further modeling revealed that a *positive* ν_{FeN}/ν_{NO} correlation stems from $Fe^{III}-N-O$ bending, which can be induced by several mechanisms, including thiolate ligation. Implications of these results for heme protein function are discussed.

Table 1. $Fe^{III}-NO$ and N−O Stretching Frequencies (cm^{-1}) for Six-Coordinate $Fe^{III}(NO)$ Complexes of Heme Proteins and Porphyrin Models

Protein/porphyrin	ν(Fe−NO)	ν(N−O)	refs
(His)$Fe^{III}(NO)$ complexes			
NOR[a]	594	1904	7
HRP[b]	604	1903	17, 18
hHO-1[c]	596	1918	19
NP1[d] (pH 8.0)	591	1917	20, 21
NP1 (pH 5.6)	591	1904	20, 21
NP4[e] (pH 7.5)	593	1921	22, 23
NP4 (pH 5.5)	590	1904	22, 23
HbN[f]	591	1914	24
HbN-Y33F[g]	592	1908	24
HbA[h]	594	1925	17
Mb[i]	594	1921	t.w.[p]
OEP(Pyr)[j]	602	1917	25, 26
(Cys)$Fe^{III}(NO)$ complexes			
$P450_{cam}$[k] (substrate free)	528	1806	27, 28
$P450_{cam}$ + camphor	522	1806	27, 28
$P450_{cam}$ + norcamphor	524	1818	27, 28
$P450_{cam}$ + adamantanone	520	1818	27
CPO[l]	538	1868	27, 28
$P450_{nor}$[m]	529	1851	28, 29
$P450_{nor}$ (proto)	530	1853	30
$P450_{nor}$ (meso)	532	1852	30
$P450_{nor}$ (deutero)	533	1851	30
SR[n]	510	1828	31
SR-HB[o]	515	1837	31

[a] Bacterial nitric oxide reductase from *Paracoccus denitrificans*. [b] Horseradish peroxidase. [c] Human heme oxygenase-1. [d] Nitrophorin 1 from *Rhodnius prolixus*. [e] Nitrophorin 4 from *Rhodnius prolixus*. [f] Truncated hemoglobin from *Mycobacterium tuberculosis*. [g] Tyrosine 33 to phenylalanine mutant of HbN. [h] Human hemoglobin. [i] Myoglobin. [j] Fe(III)-octaethylporphyrin with pyridine as proximal ligand. [k] Cytochrome P450cam. [l] Chloroperoxidase. [m] Cytochrome P450 nitric oxide reductase from *Fusarium oxysporum*. [n] Fe(III) porphyrin−alkanethiolate complex. [o] Hydrogen-bonded SR. [p] This work.

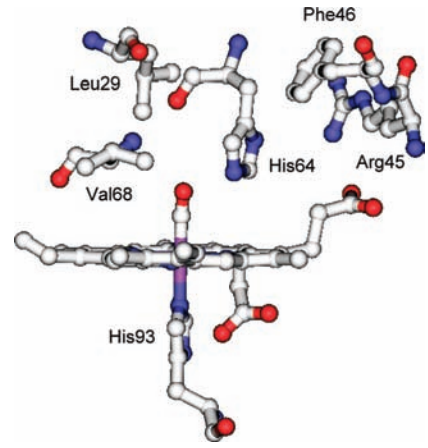

Figure 2. Structure of sperm whale $Mb^{II}(CO)$ (pdb ID: 1A6G), showing the mutated distal residues in the variants studied.

Materials and Methods

Mb Samples. Preparation of the Mb variants has been described elsewhere.[32,33] Mb samples were converted to the Fe(III) (metMb) form by adding a ca. 10-fold excess of sodium ferricyanide (Aldrich) and removing excess ferricyanide with a Sephadex G-25 PD-10 column (GE Healthcare), pre-equilibrated with 100 mM sodium phosphate, pH 7.0 buffer. $Fe^{III}(NO)$ adducts were then prepared either by passing ^{14}NO gas (Matheson Gas Products) anaerobically

(14) Phillips, J.; George, N.; Teodoro, M. L.; Li, T.; Smith, B.; Olson, J. S. *J. Phys. Chem. B* **1999**, *103*, 8817–8829.
(15) Coyle, C. M.; Vogel, K. M.; Rush, T. S., III; Kozlowski, P. M.; Williams, R.; Spiro, T. G.; Dou, Y.; Ikeda-Saito, M.; Olson, J. S.; Zgierski, M. Z. *Biochemistry* **2003**, *42*, 4896–4903.
(16) Miller, L. M.; Pedraza, A. J.; Chance, M. R. *Biochemistry* **1997**, *36*, 12199–12207.

through a 200 μL, 0.1−0.2 mM sample in a sealed NMR tube or by injecting the required amount of chemically generated ^{15}NO via an airtight syringe.

Resonance Raman Measurements. RR spectra were collected for the ν_{FeN} region using 413.1-nm excitation from a Kr^+ ion laser (Spectra Physics, 2080-RS) and for the ν_{NO} region using 244-nm excitation from an intracavity doubled-Ar^+ ion laser (Innova 300 FReD, Coherent Radiation, Palo Alto, CA). Photodissociation and reduction of the NO adducts were minimized by using low laser power (~1 mW at the sample) and by spinning the sample. For the visible RR experiments, the scattered light was collected and focused onto a triple spectrograph (Spex 1877) equipped with a CCD detector (Roper Scientific, Model 7375-0001) operating at −110 °C. Spectra were calibrated with dimethylsulfoxide-d_6. For the ultraviolet RR (UVRR) experiments, a single spectrograph (Spex 1269) equipped with a UV-enhanced CCD detector (Princeton Instruments, Model LN/CCD-1340/400) was used to collect the scattered light. UVRR spectra were calibrated using acetone and dimethylsulfoxide-d_6.

DFT Calculations. Density functional theory (DFT; B3LYP) calculations on the model complexes were performed using the Gaussian 03 program.[34] The standard 6-31G* basis set was used for all the atoms except Fe, for which Ahlrichs' valence triple-ζ (VTZ) basis set was chosen.[35] Geometry optimization and frequency calculations were performed using tight convergence criteria and an ultrafine integration grid. C_s symmetry constraints were used for the Fe^{III}(NO) porphyrin models without distal imidazole, where proximal imidazole was kept in the plane bisecting the Fe−N(pyrrole) bonds. For the models with distal imidazole, structures were optimized under C_s or no symmetry (C_1) constraints as specified for each case. Vibrational frequency values were taken directly from the Gaussian program without scaling. In all calculations, a singlet ground state for the Fe^{III}(NO) complexes was assumed.

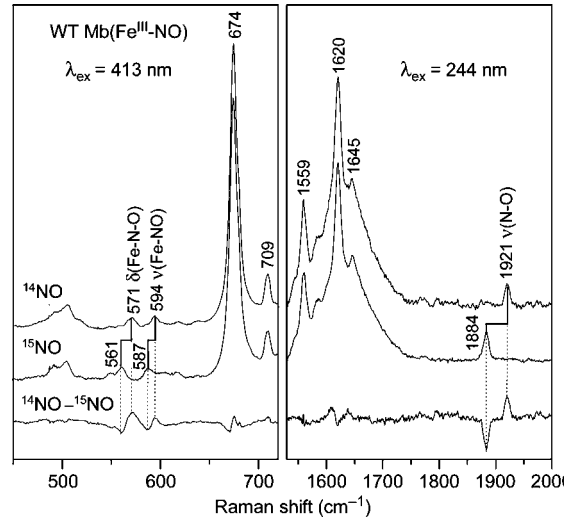

Figure 3. RR spectra for Fe^{III}(NO) adducts of wild-type Mb containing ^{14}NO or ^{15}NO, and the difference spectra (^{14}NO − ^{15}NO).

Results

Resonance Raman Spectra of Fe^{III}(NO) Mb Variants. Although a number of RR spectra for Fe^{III}(NO) heme adducts have been reported (Table 1), the data are sparse. Facile autoreduction to the more stable Fe^{II}(NO) adducts is undoubtedly responsible for the relative paucity of literature reports. Although we hoped to obtain systematic data on model complexes, as we had for Fe^{II}(CO)[12] and Fe^{II}(NO)[13,36] adducts, our efforts have been frustrated by autoreduction and high background scattering.

We have, however, obtained high quality visible and ultraviolet RR spectra of carefully prepared Fe^{III}(NO) adducts of Mb using low laser intensities. The samples included Mb variants with distal residue substitutions (Figure 2), designed to vary the electric field distribution around the bound NO.[14,37] These variations have been shown to produce systematic vibrational shifts in Fe^{II}(CO)[38] and Fe^{II}(NO)[15] adducts of Mb, and we sought similar effects for the isoelectronic Fe^{III}(NO).

RR spectra are illustrated in Figure 3 for wild-type (WT) Mb. The spectrum obtained with 413.1-nm excitation, in resonance with the heme Soret absorption, reveals the Fe^{III}−NO stretching and bending vibrations at 594 and 571 cm^{-1}, respectively, assigned[17] by the shifts induced upon substituting ^{15}NO for ^{14}NO. To detect the N−O stretching vibration, we utilized excitation at 244 nm, where enhancement of this mode occurs, probably via resonance with an Fe(III)←NO ligand-to-metal charge-transfer (LMCT) transition.[18]

Spectra of similar quality were obtained for the remaining Mb variants; some of their ^{14}NO − ^{15}NO difference spectra are displayed in Figures 4 and 5, which reveal a novel and unexpected pattern. The ν_{FeN} bands all fall in a narrow range, 590−600 cm^{-1}, but the ν_{NO} bands occupy two distinct regions, one at ~1920 cm^{-1} and one at ~1900 cm^{-1}. The common thread is that the distal histidine residue, His64, is present in the ~1920 cm^{-1} variants (Figure 4) but is replaced by hydrophobic residues

(17) Benko, B.; Yu, N.-T. *Proc. Natl. Acad. Sci. U.S.A.* **1983**, *80*, 7042–7046.
(18) Tomita, T.; Haruta, N.; Aki, M.; Kitagawa, T.; Ikeda-Saito, M. *J. Am. Chem. Soc.* **2001**, *123*, 2666–2667.
(19) Wang, J.; Lu, S.; Moenne-Loccoz, P.; Ortiz de Montellano, P. R. *J. Biol. Chem.* **2003**, *278*, 2341–2347.
(20) Maes, E. M.; Walker, F. A.; Montfort, W. R.; Czernuszewicz, R. S. *J. Am. Chem. Soc.* **2001**, *123*, 11664–11672.
(21) Ding, X.-D.; Weichsel, A.; Andersen, J. F.; Shokhireva, T. K.; Balfour, C.; Pierik, A. J.; Averill, B. A.; Montfort, W. R.; Walker, F. A. *J. Am. Chem. Soc.* **1999**, *121*, 128–138.
(22) Zaczek, M. B.; Zareba, A. A.; Czernuszewicz, R. S.; Montfort, W. R. *J. Porphyrins Phthalocyanines* **2006**, *10*, 928.
(23) Nienhaus, K.; Maes, E. M.; Weichsel, A.; Montfort, W. R.; Nienhaus, G. U. *J. Biol. Chem.* **2004**, *279*, 39401–39407.
(24) Mukai, M.; Ouellet, Y.; Ouellet, H.; Guertin, M.; Yeh, S.-R. *Biochemistry* **2004**, *43*, 2764–2770.
(25) Lipscomb, L. A.; Lee, B.-S.; Yu, N.-T. *Inorg. Chem.* **1993**, *32*, 281–286.
(26) Mu, X. H.; Kadish, K. M. *Inorg. Chem.* **1988**, *27*, 4720–4725.
(27) Hu, S.; Kincaid, J. R. *J. Am. Chem. Soc.* **1991**, *113*, 2843–2850.
(28) Obayashi, E.; Tsukamoto, K.; Adachi, S.; Takahashi, S.; Nomura, M.; Iizuka, T.; Shoun, H.; Shiro, Y. *J. Am. Chem. Soc.* **1997**, *119*, 7807–7816.
(29) Shimizu, H.; Obayashi, E.; Gomi, Y.; Arakawa, H.; Park, S.-Y.; Nakamura, H.; Adachi, S.-I.; Shoun, H.; Shiro, Y. *J. Biol. Chem.* **2000**, *275*, 4816–4826.
(30) Singh, U. P.; Obayashi, E.; Takahashi, S.; Iizuka, T.; Shoun, H.; Shiro, Y. *Biochim. Biophys. Acta* **1998**, *1384*, 103–111.
(31) Suzuki, N.; Higuchi, T.; Urano, Y.; Kikuchi, K.; Uchida, T.; Mukai, M.; Kitagawa, T.; Nagano, T. *J. Am. Chem. Soc.* **2000**, *122*, 12059–12060.
(32) Springer, B. A.; Egeberg, K. D.; Sligar, S. G.; Rohlfs, R. J.; Mathews, A. J.; Olson, J. S. *J. Biol. Chem.* **1989**, *264*, 3057–3060.
(33) Dou, Y.; Maillett, D. H.; Eich, R. F.; Olson, J. S. *Biophys. Chem.* **2002**, *98*, 127–148.
(34) Frisch, M. J.; et al. *Gaussian 03*, revision E.01; Gaussian, Inc.: Wallingford, CT, 2004.
(35) Bauernschmitt, R.; Ahlrichs, R. *Chem. Phys. Lett.* **1996**, *256*, 454–464.
(36) Ibrahim, M.; Xu, C.; Spiro, T. G. *J. Am. Chem. Soc.* **2006**, *128*, 16834–16845.
(37) Franzen, S. *J. Am. Chem. Soc.* **2002**, *124*, 13271–13281.
(38) Li, T.; Quillin, M. L.; Phillips, G. N.; Olson, J. S. *Biochemistry* **1994**, *33*, 1433–1446.

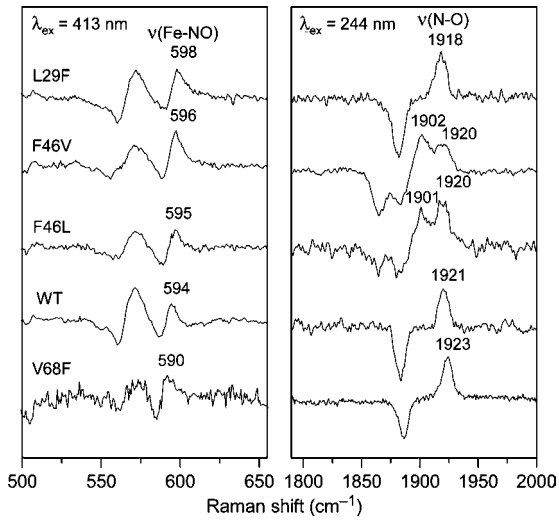

Figure 4. RR difference spectra ($^{14}NO - {}^{15}NO$) for $Fe^{III}(NO)$ adducts of the indicated Mb variants, which retain the distal His64.

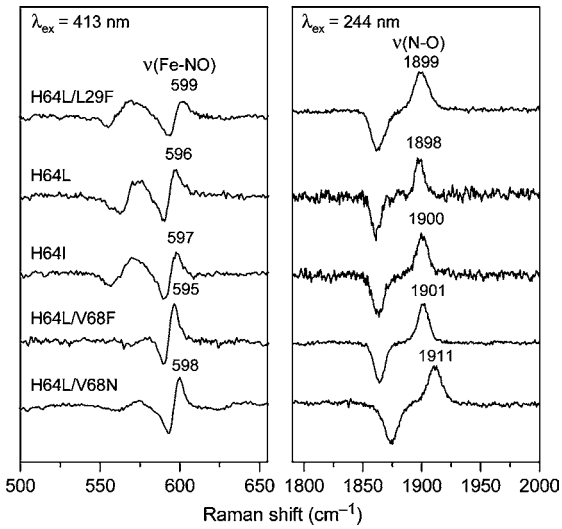

Figure 5. RR difference spectra ($^{14}NO - {}^{15}NO$) for $Fe^{III}(NO)$ adducts of the indicated Mb variants, in which distal His64 is replaced by hydrophobic residues leucine or isoleucine.

(Ile or Leu) in the ~1900 cm^{-1} variants (Figure 5). However, two of the His64-containing variants, F46L and F46V, show both ν_{NO} bands. In these variants the bulky Phe46 residue, which buttresses the His64 side chain (Figure 2), is replaced by smaller residues. Other studies have shown that this substitution increases the mobility of His64, whose side chain can occupy alternative positions, an inward conformer neighboring the heme NO ligand or an outward conformer away from it.[14,39,40] Thus, the two ν_{NO} bands in these mutants reflect populations in which His64 does or does not interact with the bound NO.

These data are listed in Table 2, along with data from additional variants (spectra in Figure S1), in which His64 is replaced by the polar residue Gln, or in which Arg45 is replaced with smaller or oppositely charged amino acids. Again the ~1900- and 1920-cm^{-1} bands show up simultaneously. The R45A and R45E substitutions eliminate an anchoring salt-bridge between Arg45 and a heme propionate and increase the mobility

Table 2. Fe^{III}−NO and N−O Stretching Frequencies (cm^{-1}) of Six-Coordinate $Fe^{III}(NO)$ Myoglobin Mutants

Mb mutant	ν(Fe−NO)	ν(N−O) (%)[a]
WT	594	1921
V68F	590	1923
F46L	595	1920 (61), 1901 (39)
F46V	596	1920 (48), 1902 (52)
L29F	598	1918
H64I	597	1900
H64L	596	1898
H64L/V68F	595	1901
H64L/L29F	599	1899
H64L/V68N	598	1911
H64Q	597	1920 (44), 1903 (56)
H64Q/V68F	594	1921 (75), 1903 (25)
H64Q/L29F	598	1919 (36), 1900 (64)
H64Q/L29F/V68F	596	1919 (82), 1901 (18)
R45A	594	1923 (81), 1905 (19)
R45E	594	1923 (75), 1905 (25)
R45K	594	1922

[a] For Mb variants with two ν_{NO} frequencies, the percentage area for each band is shown in parentheses.

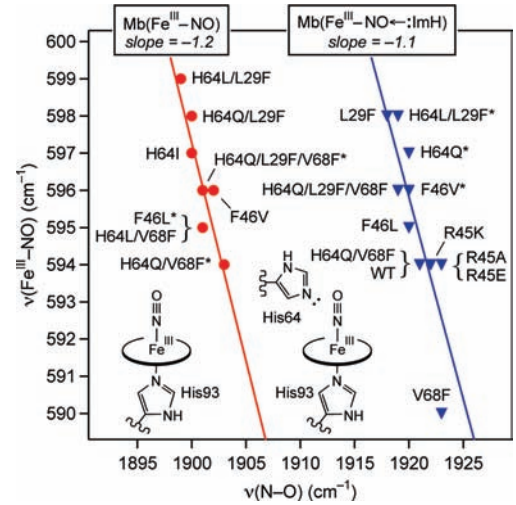

Figure 6. ν_{FeN}/ν_{NO} data for $Fe^{III}(NO)$ adducts of the indicated Mb variants, without (●) and with (▼) lone-pair donation to the bound NO from a distal His64 or Gln64. Asterisks indicate minor components when two ν_{NO} populations are detected. The red and blue lines are linear correlations with $r = 0.88$ and 0.84, respectively.

of His64,[14,41,42] thus accounting for the two populations. In the R45K variant, this salt-bridge is preserved by the positively charged Lys45, and only the WT-like population is seen. For the H64Q variants, we infer that there are again two populations, this time with Gln64 interacting or not with the bound NO, in the same manner as His64. The Gln64 side chain can donate a lone pair from the carbonyl O^{ϵ} atom but is expected to be more mobile than that of His64.

When ν_{FeN} is plotted against ν_{NO} (Figure 6), it is apparent that there are *two* parallel correlations (solid lines), one in which His64 or Gln64 interacts with the NO, and one in which this interaction is absent. Both correlations are negative, as expected for backbonding, and the values of the slopes, −1.1 and −1.2, respectively, are somewhat larger than those observed when ν_{FeC}

(39) Olson, J. S.; Phillips, G. N. *J. Biol. Inorg. Chem.* **1997**, *2*, 544–552.
(40) Lai, H. H.; Li, T.; Lyons, D. S.; Phillips, G. N. J.; Olson, J. S.; Gibson, Q. H. *Proteins: Struct., Funct., Genet.* **1995**, *22*, 322–339.
(41) Harada, K.; Makino, M.; Sugimoto, H.; Hirota, S.; Matsuo, T.; Shiro, Y.; Hisaeda, Y.; Hayashi, T. *Biochemistry* **2007**, *46*, 9406–9416.
(42) Carver, T. E.; Olson, J. S.; Smerdon, S. J.; Krzywda, S.; Wilkinson, A. J.; Gibson, Q. H.; Blackmore, R. S.; Ropp, J. D.; Sligar, S. *Biochemistry* **1991**, *30*, 4697–4705.

Table 3. Selected Bond Lengths (Å), Bond Angles (deg), and Vibrational Stretching Frequencies (cm^{-1}) Calculated for Six-Coordinate (ImH)Fe^{III}(NO), (ImH)Fe^{III}(NO)···(ImH), and (ImH)Fe^{III}(NO)···(H_2O) Adducts[a]

Complex	Fe−NO	N−O	∠FeNO	Fe−N_{Im}^{p}	$N_{NO}\cdots N_{Im}^{d}$	$O_{NO}\cdots N_{Im}^{d}$	ν(Fe−NO)	ν(N−O)
(ImH)−Fe^{III}−NO, C_s symmetry								
$FeP(NH_2)_8$	1.630	1.138	178.4	2.027	−	−	666	2057
$FeP(CH_3)_8$	1.632	1.137	179.7	2.025	−	−	666	2063
FeP	1.636	1.136	179.8	2.020	−	−	660	2070
$FePF_8$	1.642	1.134	179.8	2.019	−	−	649	2077
$FePCl_8$	1.643	1.133	179.8	2.014	−	−	647	2079
$FeP(NO_2)_8$	1.656	1.130	179.9	2.005	−	−	629	2092
(ImH)−Fe^{III}−NO←:N(ImH), C_s symmetry								
$FeP(NH_2)_8$	1.642	1.132	175.4	2.026	3.454	2.855	650	2084
$FeP(CH_3)_8$	1.645	1.131	175.3	2.023	3.426	2.832	647	2088
FeP	1.650	1.130	175.8	2.020	3.401	2.777	639	2096
$FePF_8$	1.657	1.128	177.3	2.019	3.353	2.706	626	2103
$FePCl_8$	1.660	1.127	177.2	2.014	3.346	2.685	623	2104
$FeP(NO_2)_8$	1.683	1.126	178.5	2.005	3.264	2.535	575	2101
(ImH)−Fe^{III}−NO←:N(ImH), C_1 symmetry								
$FeP(NH_2)_8$	1.638	1.133	176.1	2.028	3.351	2.966	656	2080
$FeP(CH_3)_8$	1.642	1.132	174.5	2.025	3.238	2.929	650	2085
FeP	1.648	1.131	172.2	2.021	3.118	2.920	641	2089
$FePF_4$	1.654	1.130	169.4	2.019	3.010	2.921	627	2088
$FePF_8$	1.662	1.130	166.8	2.016	2.922	2.917	609	2083
$FePCl_8$	1.672	1.130	163.4	2.010	2.794	2.897	587	2072
$FeP(NO_2)_8$	1.713	1.131	156.0	2.003	2.529	2.797	519	2041
(ImH)−Fe^{III}−NO←(:OH_2), C_1 symmetry								
FeP	1.647	1.131	173.4	2.020	2.949	2.807	644	2092
(ImH)−Fe^{III}−NO←(:OH_2)$_2$, C_1 symmetry								
FeP	1.655	1.126	174.6	2.022	2.97/3.12	2.74/2.78	635	2117
(ImH)−Fe^{III}PH−NO, Constrained ∠Fe^{III}NO, C_s symmetry								
FeP	1.755	1.146	140	1.981	−	−	440	1938
FeP	1.701	1.141	150	1.989	−	−	505	1993
FeP	1.664	1.138	160	2.002	−	−	594	2036
FeP	1.643	1.136	170	2.014	−	−	645	2062
FeP	1.641	1.136	172	2.017	−	−	649	2065
FeP	1.639	1.136	174	2.018	−	−	657	2067

[a] N_{Im}^{p} and N_{Im}^{d} are the nitrogen atoms of proximal and distal imidazoles, respectively (see Figure 9).

is plotted against ν_{CO} for Fe^{II}(CO) adducts, −0.73.[43] Side chain substitutions that increase the positive polarity near the bound NO, e.g., via the Phe multipole in L29F,[44] shift the point higher on either line.

DFT Modeling. Density functional theory was used to analyze trends in structure and vibrational frequencies for Fe^{III}(NO) heme adducts. The basic model was (ImH)Fe^{III}(NO)P, where ImH is imidazole and P is porphine. The level of theory was the same (see Material and Methods section) as was used successfully for Fe^{II}(CO) adducts.[36] The calculated structure (see bond parameters for FeP in Table 3) agrees well with those reported by others,[8,10,45] using different levels of theory, and also with available model complex crystallographic data.[46,47] No Mb^{III}(NO) crystal structure is available, but EXAFS analysis[48] has indicated a linear Fe^{III}−N−O unit and bond distances consistent with the models.

The computed ν_{FeN} and ν_{NO} frequencies, 660 and 2070 cm^{-1}, are overestimated, as is usually the case with DFT, for which empirical scaling factors are often applied.[49−51] The required scaling factor for ν_{NO}, ∼0.92, is indeed the same as that determined by Pulay and co-workers[50] and consistent with the range generally encountered for molecules of the first row elements.[51] Scaling factors for metal−ligand bonds have not been collected. Since we are interested in frequency trends, and not in absolute values, we have not applied scaling factors.

(a) Inductive Effects of Peripheral *β*-Substituents. To examine the effects of backbonding, we resorted to the same method as that employed previously for Fe^{II}(CO)[12,36] and Fe^{II}(NO)[36] adducts, attaching electron-donating or -withdrawing substituents to the porphine periphery. Electron donors are expected to increase backdonation to the axial ligand, via their inductive effect, while electron-withdrawing substituents should decrease backdonation. This computational device has been applied to (ImH)Fe^{III}(NO)P by Linder and Rodgers,[10] who found a *positive* correlation of ν_{FeN} and ν_{NO}, contrary to the negative correlation expected for backbonding. However, the positive correlation was based on a set of substituents attached to the *meso*-carbon atoms of porphine (Figure 7). Their calculations for substituents attached to the β-carbon atoms did not follow this correlation, and indeed the β-substituent points appeared to be negatively correlated.

(43) Spiro, T. G.; Wasbotten, I. H. *J. Inorg. Biochem.* **2005**, *99*, 34–44.
(44) Carver, T. E.; Brantley, R. E.; Singleton, E. W.; Arduini, R. M.; Quillin, M. L.; Phillips, G. N.; Olson, J. S. *J. Biol. Chem.* **1992**, *267*, 14443–14450.
(45) Wondimagegn, T.; Ghosh, A. *J. Am. Chem. Soc.* **2001**, *123*, 5680–5683.
(46) Ellison, M. K.; Scheidt, W. R. *J. Am. Chem. Soc.* **1999**, *121*, 5210–5219.
(47) Ellison, M. K.; Schulz, C. E.; Scheidt, W. R. *J. Am. Chem. Soc.* **2002**, *124*, 13833–13841.
(48) Rich, A. M.; Armstrong, R. S.; Ellis, P. J.; Lay, P. A. *J. Am. Chem. Soc.* **1998**, *120*, 10827–10836.
(49) Rauhut, G.; Pulay, P. *J. Phys. Chem.* **1995**, *99*, 3093–3100.
(50) Rauhut, G.; Jarzecki, A. A.; Pulay, P. *J. Comput. Chem.* **1997**, *18*, 489–500.
(51) Merrick, J. P.; Moran, D.; Radom, L. *J. Phys. Chem. A* **2007**, *111*, 11683–11700.

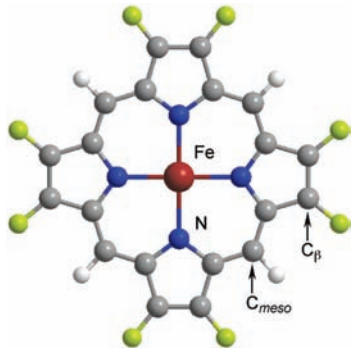

Figure 7. Fe porphine with eight substituents on the β-carbon atoms.

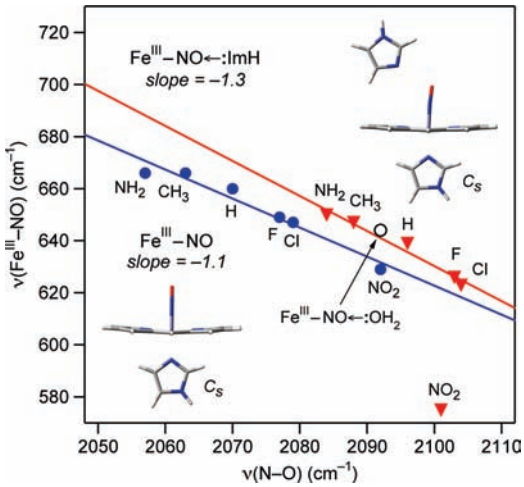

Figure 8. ν_{FeN}/ν_{NO} correlation plots computed for the six-coordinate (ImH)Fe^{III}(NO)PX_8 complexes, without (blue points) and with a distal ImH, held in C_s symmetry (red triangles). "○" indicates (ImH)Fe^{III}(NO)P with a distal water molecule. Linear correlations are shown for models without distal ImH (blue line, $r = 0.98$) and with distal ImH in C_s symmetry (red line, $r = 0.98$), but excluding the $-NO_2$ data point.

For Fe^{II}(CO) adducts the position of substitution does not materially affect the slope of the ν_{FeC}/ν_{CO} correlation,[36] but for Fe^{III}(NO) there is a specific electronic effect of *meso*-substituents, because of an altered orbital energy structure, as discussed below. Consequently, we limited the position of substitution to the β-carbon atoms. Table 3 lists structures and frequencies for (ImH)Fe^{III}(NO)P with eight β-substituents, $-NH_2$, $-CH_3$, $-H$, $-F$, $-Cl$, and $-NO_2$, arranged from the most donating to the most withdrawing. The resulting ν_{FeN}/ν_{NO} correlation (Figure 8) gives a straight line with a slope of -1.1, in excellent agreement with the experimental correlations found for the Mb^{III}(NO) adducts. Thus, the experimental data behave according to the backbonding model.

(b) Distal Imidazole Interaction. Next we modeled the effect of a distal histidine interaction, by placing an imidazole ring near the bound NO ligand. In the first set of calculations, the distal ImH was restricted to the same plane as the proximal ImH, which bisected the Fe−N(pyrrole) bonds (C_s overall symmetry, Figure 9a).

The distal ImH was initially placed with its N−H proton pointing at the NO, simulating H-bonding. This orientation is stable for Fe^{II}(CO)[37,52−54] and Fe^{II}(NO)[55,56] adducts, but for

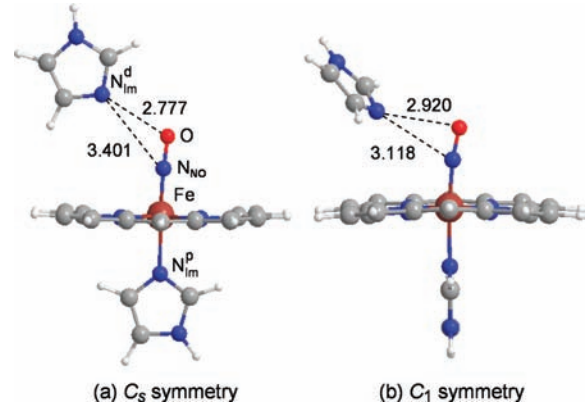

Figure 9. DFT-optimized molecular structures and atom labeling for (ImH)Fe^{III}(NO)P with a distal ImH held in C_s symmetry (a) or allowed to relax to C_1 (b).

(ImH)Fe^{III}(NO)P no stable structure could be found with this orientation. However, a stable structure *was* found when the imidazole N: lone pair was oriented toward the NO (Figure 9a). The imidazole ring was canted to one side of the NO, but the (ImH)N: atom was much closer to the O_{NO} than the N_{NO} atom, 2.78 vs 3.40 Å (Table 3).

This stable structure supports the suggestion advanced some time ago by Miller et al.[16] that the distal His64 in Mb engages in a lone-pair donor interaction with Fe^{III}(NO). Their suggestion was based on the observation, confirmed in the present work, that the ν_{NO} (measured via FTIR spectroscopy at $\leq$40 K to prevent autoreduction; ν_{FeN} was not reported[16]) shifted down when His64 was replaced by a hydrophobic residue, whereas an upshift would have been the direction expected on the basis of backbonding, if His64 exerts positive polarity, as it does for Fe^{II}(CO).[9,14]

Next we computed structures and frequencies for β-substituted porphines, with the distal ImH in the same C_s symmetry orientation (Figure 9a). The imidazole N: moves farther from the O_{NO} atom as the substituents become more electron-donating, and the Fe^{III}−N−O unit bends slightly, in the direction away from the distal imidazole (Table 3). The N−O distance increases while the Fe−NO distance decreases, as expected from increased backbonding.

The computed frequencies now fall on a new ν_{FeN}/ν_{NO} correlation (*slope* $= -1.3$), nearly parallel to the model without a distal ImH, and are displaced $\sim$20 cm^{-1} to higher ν_{NO} values (Figure 8). Thus, the pattern observed for the Mb^{III}(NO) variants (Figure 6) is reproduced remarkably well. For a given porphyrin, the effect of the distal imidazole is to increase ν_{NO} and decrease ν_{FeN} (Table 3). Qualitatively, this effect is consistent with decreased backbonding, but the ν_{NO} increase is more pronounced, producing the observed shift in the correlation. (We note that agreement with experiment is inexact in that the Mb data indicate *no* effect of the distal imidazole on ν_{FeN}. For variants in which the distal His is mobile, two values of ν_{NO} are observed, but only one ν_{FeN}.)

What accounts for the shifted correlation? Figure 10 compares selected occupied molecular orbitals, computed for the distal imidazole model in C_s symmetry. The two orbitals on the left, HOMO−3 and −4, are the nearly degenerate pair that describes

(52) Sigfridsson, E.; Ryde, U. *J. Biol. Inorg. Chem.* **1999**, *4*, 99–110.
(53) Rovira, C.; Schulze, B.; Eichinger, M.; Evanseck, J. D.; Parrinello, M. *Biophys. J.* **2001**, *81*, 435–445.
(54) Sigfridsson, E.; Ryde, U. *J. Inorg. Biochem.* **2002**, *91*, 101–115.
(55) Xu, C.; Spiro, T. G. *J. Biol. Inorg. Chem.* **2008**, *13*, 613–621.
(56) Tangen, E.; Svadberg, A.; Ghosh, A. *Inorg. Chem.* **2005**, *44*, 7802–7805.

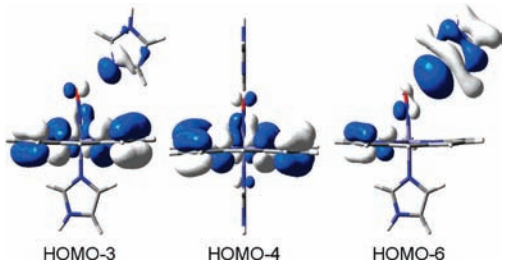

Figure 10. Selected HOMOs of the (ImH)N:→(NO)Fe^{III}(ImH) porphine model (C_s).

$Fe^{II}-NO^+$ backbonding and are similar to the backbonding orbitals in the absence of a distal imidazole. There is bonding overlap between Fe d_π and NO π^* orbitals, and an antibonding interaction with the imidazole lone pair, that inhibits backbonding. These orbitals account for the negative slope of the ν_{FeN}/ν_{NO} correlation. The orbital on the right, HOMO−6, describes an imidazole lone-pair interaction, mainly with the NO π^* orbital, with some involvement of π orbitals on the porphine, on the side opposite the distal imidazole. The imidazole lone pair pushes electrons out of the NO π^* orbital onto the porphine, thereby strengthening the N−O bond, with little effect on the $Fe^{III}-NO$ bond. This interaction is the likely origin of the shift of the ν_{FeN}/ν_{NO} correlation to higher ν_{NO} when the distal imidazole interacts mainly with the O atom of NO.

We note that the ν_{FeN}/ν_{NO} point for distal imidazole interacting with the NO_2-substituted porphine deviates from the general pattern, falling distinctly below the line for the other models (Figure 8). This deviation for the most electron-withdrawing substituent can be traced to HOMO−6 acquiring more Fe−NO antibonding character (data not shown) when the substituents are $-NO_2$, moving above the backbonding orbitals, thereby governing the $Fe^{III}-N-O$ bonding.

(c) O- versus N-Directed Imidazole and $Fe^{III}-N-O$ Bending. In the course of computing vibrational frequencies, we noted that the C_s distal imidazole model yielded a negative frequency, ~ -16 cm^{-1}, corresponding to rotation of the distal imidazole ring out of the plane to which it was constrained. While the negative frequency was low enough to preclude significant errors in the computed ν_{NO} and ν_{FeN} values, it did signal that the C_s constraint imposed an energy penalty, probably due to nonbonded contacts between the imidazole CH and the porphine macrocycle. At the close distance required for the N: lone-pair interaction, this contact is within the sum of van der Waals radii ($\sim$3 Å).

When the C_s constraint was removed, the distal imidazole rotated out of the plane, as expected. In addition, however, it shifted toward the N atom of the NO (Table 3 and Figure 9b). The imidazole N: was now only slightly closer to the O_{NO} than the N_{NO} atom, 2.92 vs 3.12 Å. Moreover, electron-withdrawing substituents pulled the (ImH)N: closer to the N_{NO} than the O_{NO} atom. They also induced significant $Fe^{III}-N-O$ bending. In the extreme case of eight $-NO_2$ substituents, the distances of (ImH)N: to O_{NO} and N_{NO} were 2.80 and 2.53 Å, respectively, while the $Fe^{III}-N-O$ angle was reduced to 156° (Table 3).

When the computed frequencies were placed on the ν_{FeN}/ν_{NO} plot (Figure 11), a surprising pattern emerged. The data for the more electron-donating β-substituents ($-NH_2$, $-CH_3$, $-H$) fall on a shifted backbonding correlation (Figure 11, top red line), similar to that found for the C_s model (Figure 11, blue line), but the data for the more electron-withdrawing β-substituents ($-F$, $-Cl$, $-NO_2$) fall on a *positive* correlation,

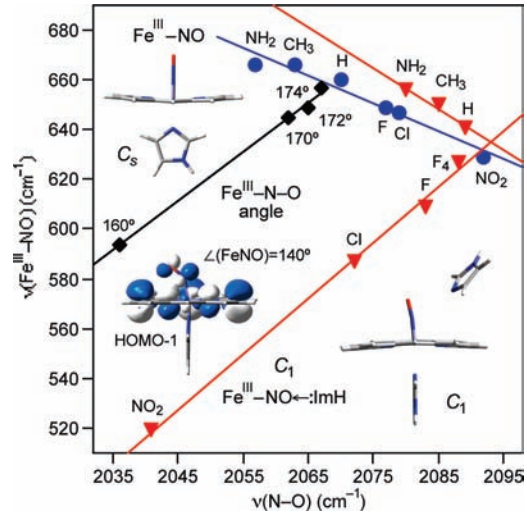

Figure 11. ν_{FeN}/ν_{NO} correlation plots computed for the (ImH)Fe^{III}(NO)PX_8 and (ImH)Fe^{III}(NO)PH_4F_4 complexes, without (blue points, data from Figure 8) and with a distal ImH allowed to relax to C_1 symmetry (red triangles). The black line is the positive correlation of ν_{FeN} and ν_{NO}, obtained by constraining the $Fe^{III}-N-O$ angle at the indicated values in the (ImH)Fe^{III}(NO)P model. Also shown is the HOMO−1 a_{2u}-type orbital for the (ImH)Fe^{III}(NO)P model with the $\angle Fe^{III}-N-O = 140°$ (electron density has been removed from the front side of the molecule, to show the Fe−N−O contribution).

both ν_{NO} and ν_{FeN} decreasing as the substituents became more electron-withdrawing (Figure 11, bottom red line). The break between the two correlations occurs between eight −H substituents (porphine) and four each of −F and −H substituents (H- and F_4-labeled points in Figure 11). With more electron-donating β-substituents the (ImH)N: stays farther from the N_{NO} than the O_{NO} atom, and the $Fe^{III}-N-O$ unit stays nearly linear, while with more electron-withdrawing β-substituents the (ImH)N: moves closer to the N_{NO} than the O_{NO} atom, and the $Fe^{III}-N-O$ unit bends strongly (Table 3).

A similar effect of the distal (ImH)N:→N_{NO} interaction was observed by constraining the distance between the distal ImH and N_{NO} at fixed values for unsubstituted Fe^{III}(NO) porphine (C_1 model). The closer the approach of the distal ImH to the N atom of NO, the more bent the $Fe^{III}-N-O$ angle became, reaching 154° at a 2.4 Å distance. The $Fe^{III}-NO$ and N−O bond lengths increased in concert as the distal (ImH)N:→N_{NO} distance decreased (Table S1, Figure S2). We note that the energy well for the interaction is shallow; only 0.4 kcal/mol are lost on increasing the $N_{NO}\cdots N_{Im}{}^d$ distance from the bottom of the well, 3.1 Å, to 3.5 Å. When the distal ImH was constrained to interact with O_{NO} (C_s model), the $Fe^{III}-N-O$ unit remained nearly linear (Table S2, Figure S3).

The positive ν_{FeN}/ν_{NO} correlation implies an effect that overrides backbonding and that correlates with $Fe^{III}-N-O$ bending. To test the role of bending *per se*, we examined its effect on the porphine model, (ImH)Fe^{III}(NO)P, by constraining the $Fe^{III}-N-O$ angle to different values (Table 3). Bending $Fe^{III}-N-O$ reduced both ν_{NO} and ν_{FeN}, producing a positive correlation (Figure 11, black line); a similar effect of bending was reported by Linder and Rodgers.[10] Indeed, the slope of the bending correlation is the same as that produced by increasingly electron-withdrawing β-substituents (Figure 11, bottom red line). We note that a positive correlation was earlier computed for the $Fe^{II}-CO$ adduct, (ImH)Fe^{II}(CO)P, upon bending the

$Fe^{II}-C-O$ unit.[57] In both cases bending weakens the Fe−N(C) and N(C)−O bonds simultaneously.

The reason for this mutual weakening can be seen in the composition of the HOMO−1 molecular orbital, shown in Figure 11 (inset) for $(ImH)Fe^{III}(NO)P$ when $Fe^{III}-N-O$ is bent. Bending induces an *antibonding* combination of the d_{xz} and π^*_{NO} orbitals, a feature noted earlier by Linder and Rodgers.[10] It is this antibonding combination that produces simultaneous Fe^{III}−NO and N−O bond weakening and a positive ν_{FeN}/ν_{NO} correlation.

In addition, bending induces interaction of π^*_{NO} with the porphyrin a_{2u}-type orbital (Figure 11, inset). The a_{2u} orbital is concentrated on the pyrrole N atoms and the *meso*-C atoms and is strongly affected by *meso*-substituents. As these substituents become electron-donating, the $a_{2u}-\pi^*_{NO}$ interaction becomes more favorable, inducing more $Fe^{III}-N-O$ bending, thereby accounting for the positive ν_{FeN}/ν_{NO} correlation computed by Linder and Rogers when the *meso*-substituents were varied. However, the a_{2u} orbital has no amplitude at the β-carbon atoms of the pyrrole rings. Consequently, β-substituents do not induce $Fe^{III}-N-O$ bending. Instead their inductive effect shifts the extent of Fe^{III}−NO backbonding, producing a negative ν_{FeN}/ν_{NO} correlation.

(d) Distal Water Interaction. Models were also constructed in which the distal imidazole was replaced by water molecules, to investigate a possible distal water effect on ν_{FeN}/ν_{NO} values of the nitrosyl ferriheme protein nitrophorin 4 (see below). Stable structures were found with the water O atoms pointing at the bound NO, somewhat closer to the O_{NO} than the N_{NO} atom (Table 3), with the $Fe^{III}-N-O$ unit remaining nearly linear. As with the distal imidazole lone pair interacting with O_{NO}, the effect of the interaction was to decrease ν_{FeN} but increase ν_{NO}, shifting the ν_{FeN}/ν_{NO} point above the interaction-free backbonding line. The H_2O effect was qualitatively similar, placing the frequency point on the correlation line formed by the models with distal (ImH)N:→O_{NO} interaction (Figure 8).

We note that Linder and Rodgers also found a stable structure for a formaldehyde molecule interacting with the bound NO in $(CH_3S^-)Fe^{III}(NO)P$, modeling the interaction of a peptide carbonyl in the enzyme cytochrome P450 nitric oxide reductase ($P450_{nor}$).[58] As the contact distance was decreased, the computed Fe^{III}−NO and N−O bond distances both decreased slightly, suggesting a positive ν_{FeN}/ν_{NO} correlation with variable interaction strength. This effect had been observed earlier by Scheidt and co-workers in crystal polymorphs of $[Fe^{III}(OEP)NO]ClO_4$ (OEP = octaethylporphyrin) having the perchlorate counterion at different distances from the NO.[11,59] Both ν_{FeN} and ν_{NO} increased for the closer counterion contact.

Discussion

$Fe^{III}(NO)$ Backbonding and Bending. Our RR spectroscopic and DFT modeling results establish that, in the absence of forces that induce bending, backbonding dominates the behavior of $Fe^{III}(NO)$ adducts, consistent with the $Fe^{II}(NO^+)$ formulation of its electronic structure. A negative ν_{FeN}/ν_{NO} correlation is found, experimentally and computationally, for NO adducts of imidazole-ligated Fe(III) heme. The slope of the correlation is essentially the same whether the backbonding is varied by electron-donating or -withdrawing porphyrin β-substituents (computation, *slope* = −1.1) or by the protein electrostatic field (experiment, *slope* = −1.2). In addition, lone-pair donation from a distal imidazole shifts the correlation to higher ν_{NO} values. This effect, seen experimentally in $Mb^{III}(NO)$ variants, is accurately modeled via DFT and is attributable to a specific orbital interaction that strengthens the N−O bond, with little effect on the Fe−NO bond.

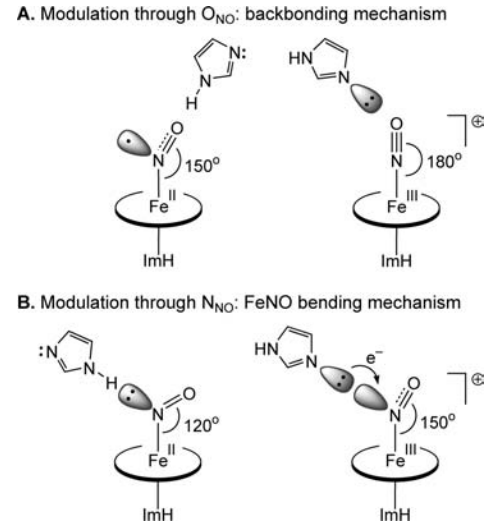

Figure 12. Different mechanisms of bond strength modulation through interaction with a distal imidazole lone pair (Fe^{III}−NO adducts) or a distal imidazole H-bond (Fe^{II}−NO adducts). (A) Modulation through the O_{NO} polarization (backbonding). (B) Modulation through interaction with N_{NO} (Fe−N−O bending).

However, $Fe^{III}(NO)$ bending overrides the backbonding anticorrelation and produces a positive ν_{FeN}/ν_{NO} correlation as the Fe−N−O angle is varied. This effect arises from induction of an antibonding combination of d_{xz} and π^*_{NO} orbitals in HOMO−1 as $Fe^{III}(NO)$ bends, resulting in simultaneous weakening of the Fe−NO and N−O bonds. Bending can result from a distal lone-pair donor that is drawn close enough to interact with the N instead of the O atom of the NO.

There are interesting parallels between distal lone-pair interactions with $Fe^{III}(NO)$ adducts and distal H-bond interactions with $Fe^{II}(NO)$ adducts, investigated earlier,[36,55] which can best be appreciated with the aid of the valence bond diagrams in Figure 12. In both cases, interaction at the O_{NO} atom polarizes the π bonds. Backbonding is enhanced by H-bonding to $Fe^{II}(NO)$ but diminished by lone-pair donation to $Fe^{III}(NO)$, which, in addition, strengthens the N−O bond via a specific orbital interaction. In both Fe oxidation states, interaction at the N_{NO} atom pulls the electron density into the sp^2-like antibonding orbital, inducing bending and weakening both the Fe−NO and N−O bonds.

For $Fe^{II}(NO)$, DFT computation reveals stable H-bond interactions at either O_{NO} or N_{NO}, depending on the disposition of the H-bond donor.[55,56] Examples of both interactions are found in different heme proteins (see ref 55 and references therein). For $Fe^{III}(NO)$, the preferred lone-pair interaction is with O_{NO}, unless the donor is drawn toward the N_{NO} by electron-withdrawing heme β-substituents, or unless the donor is a strong nucleophile, like a hydroxide ion (see below). Since protoporphyrin IX does not have electron-withdrawing substituents, and since protein side chains are not strong nucleophiles, the

(57) Kozlowski, P. M.; Vogel, K. M.; Zgierski, M. Z.; Spiro, T. G. *J. Porphyrins Phthalocyanines* **2001**, *5*, 312–322.
(58) Linder, D. P.; Rodgers, K. R. *J. Biol. Inorg. Chem.* **2007**, *12*, 721–731.
(59) Ellison, M. K.; Schulz, C. E.; Scheidt, W. R. *Inorg. Chem.* **2000**, *39*, 5102–5110.

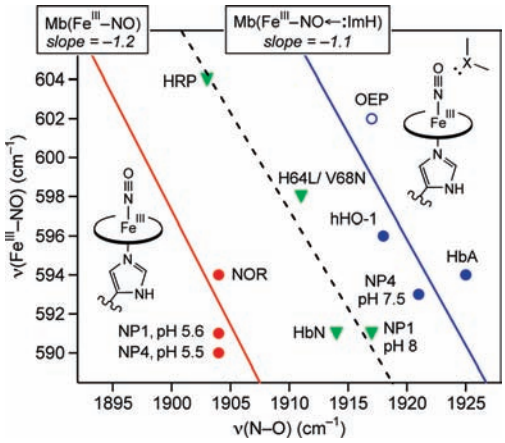

Figure 13. ν_{FeN}/ν_{NO} data for the indicated His-ligated $Fe^{III}(NO)$ heme proteins, which fall on the plus (blue line) or minus (red line) distal His lines of $Mb^{III}(NO)$ variants shown in Figure 6 or form a parallel intermediate linear correlation (dashed line with $r = 0.96$ and *slope* $= -1.0$). NOR = nitric oxide reductase, hHO-1 = human heme oxygenase-1, HbA = human hemoglobin, HbN = truncated hemoglobin with distal Tyr and Gln residues, NP4 = nitrophorin 4 and NP1 = nitrophorin 1 at the indicated pH values, HRP = horseradish peroxidase, and H64L/V68N = His64Leu/Val68Asn Mb double mutant. Pyridine adduct of a model complex $Fe^{III}OEP(NO)$ (OEP = octaethylporphyrin) is also shown (○).

$Fe^{III}(NO)$ structural and vibrational data from ferriheme nitrosyls can be interpreted in terms of backbonding and lone-pair interactions with O_{NO}, provided the proximal ligand is histidine.

Implications for Imidazole-Ligated Ferriheme Nitrosyls. With the ν_{FeN}/ν_{NO} correlations established for $Mb^{III}(NO)$, we can interpret reported vibrational data for $Fe^{III}(NO)$ adducts of other imidazole-ligated proteins and models (Figure 13). The extensively characterized nitrophorins from the saliva of the "kissing" bug *Rhodnius prolixus* are of particular interest, because of the stability of their $Fe^{III}(NO)$ adducts. Two sets of $Fe^{III}(NO)$ stretching frequencies have been reported for nitrophorin 4 (NP4), at pH 7.5 and 5.5.[22] Intriguingly, these fall on the two lines described by $Mb^{III}(NO)$ variants, with and without distal imidazole interactions. At the lower pH, NP4 is in a "closed" form in which hydrophobic residues are packed around the bound NO. There is no potential lone-pair donor, and the ν_{FeN}/ν_{NO} (590/1904 cm^{-1}) position, at the low end of the imidazole-less backbonding line (Figure 13, red line), indicates an environment of low polarity.

An early crystal structure of the $Fe^{III}(NO)$ adduct of NP4 at pH 5.6 was refined as two conformers, one with a linear and one with a severely bent (110°) Fe−N−O unit.[60] The severely bent conformation was later attributed to partial reduction to $Fe^{II}(NO)$ in the X-ray beam, and a higher resolution gave a single conformer with ∠Fe−N−O = 156°, but with thermal disorder at the O position.[61] It seems likely that this determination too was influenced by X-ray-induced reduction, since the ν_{FeN}/ν_{NO} data would have shown a pronounced deviation below the backbonding line for this degree of bending (see Figure 11), and this is not observed.

At pH 7.5, a conformational change in NP4 induces disorder in a pair of loops lining the bound NO and opens the distal heme pocket to solvent. The ν_{FeN}/ν_{NO} data (593/1921 cm^{-1}) place this form on the distal lone-pair line (Figure 13, blue line), yet there is no distal histidine or any other potential donor side chain on the distal side of the heme; an aspartate residue is ~6 Å from the Fe,[61] too far to donate an electron pair, though it could polarize an intervening water molecule. The actual ferriheme−NO structure is not available at pH 7.5, because of instability to X-ray-induced reduction, but crystal structures of NH_3 and CN^- adducts reveal an open, water-filled distal pocket.[60–62] In the CN^- adduct, a distal threonine residue orients a water molecule, holding it 2.5 Å from CN^- (pdb ID: 1EQD). Our DFT modeling indicates that a lone-pair donating water molecule could have an effect on ν_{FeN}/ν_{NO} equivalent to a distal imidazole (Table 3 and Figure 8).

Like NP4, nitrophorin 1 (NP1) has an open binding pocket at elevated pH, but the crystal structure of the NP1(CN^-) adduct (pdb ID: 3NP1) shows fewer water molecules than in NP4(CN^-), and none are localized to the immediate vicinity of the CN^-, in contrast to NP4(CN^-) (pdb ID: 1EQD). Consistent with this difference, the ν_{FeN}/ν_{NO} data point for NP1(NO) at pH 8.0[20,21] is shifted to an intermediate position (Figure 13, dashed line), indicating a weaker lone-pair donor interaction.

Human heme oxygenase-1 (hHO-1)[19] falls on the distal imidazole line (Figure 13, blue line), but in this case the lone-pair donor is the carbonyl oxygen of distal Gly139, which the crystal structure shows to be in close contact with bound NO, as seen in the $Fe^{II}(NO)$ adduct (3.1 and 2.7 Å distances to N_{NO} and O_{NO}, respectively).[63] Reported data for the pyridine adduct of $Fe^{III}OEP(NO)$[25,26] also fall on the distal imidazole line, indicating that excess pyridine, present to ensure adduct formation, provided a lone-pair interaction.

In nitric oxide reductase (NOR) from *Paracoccus denitrificans*, a cytochrome *bc* protein, NO binds to a vacant coordination site on imidazole-ligated ferriheme b_3.[64,65] Spectroscopic studies indicate that a trisimidazole-ligated non-heme Fe_B is distal to the heme b_3 in NOR,[66] analogous to the Cu_B center in cytochrome *c* oxidase (C*c*O),[67–69] and is likely involved in NO reduction. A model complex has been synthesized, and interestingly, its $Fe^{III}(NO)$ vibrational frequencies,[70] ν_{FeN}/ν_{NO} = 610/1924 cm^{-1}, place it far above the $Mb^{III}(NO)$ correlations in Figure 13. This placement is reminiscent of the elevated ν_{FeC}/ν_{CO} frequencies found for the CO adduct of C*c*O.[71,72] In that case, a compression effect of the heme/Cu_B dinuclear site was invoked to explain the elevated ν_{FeC},[43] and a similar explanation may apply to the NOR model. However, NOR itself does not

(60) Weichsel, A.; Andersen, J. F.; Roberts, S. A.; Montfort, W. R. *Nat. Struct. Biol.* **2000**, *7*, 551–554.
(61) Roberts, S. A.; Weichsel, A.; Qiu, Y.; Shelnutt, J. A.; Walker, F. A.; Montfort, W. R. *Biochemistry* **2001**, *40*, 11327–11337.
(62) Kondrashov, D. A.; Roberts, S. A.; Weichsel, A.; Montfort, W. R. *Biochemistry* **2004**, *43*, 13637–13647.
(63) Lad, L.; Wang, J.; Li, H.; Friedman, J.; Bhaskar, B.; Ortiz de Montellano, P. R.; Poulos, T. L. *J. Mol. Biol.* **2003**, *330*, 527–538.
(64) Wasser, I. M.; De Vries, S.; Moenne-Loccoz, P.; Schroder, I.; Karlin, K. D. *Chem. Rev.* **2002**, *102*, 1201–1234.
(65) Zumft, W. G. *Microbiol. Mol. Biol. Rev.* **1997**, *61*, 533–616.
(66) Moenne-Loccoz, P.; Richter, O.-M. H.; Huang, H.; Wasser, I. M.; Ghiladi, R. A.; Karlin, K. D.; de Vries, S. *J. Am. Chem. Soc.* **2000**, *122*, 9344–9345.
(67) Scott, R. A. *Annu. Rev. Biophys. Biophys. Chem.* **1989**, *18*, 137–158.
(68) Powers, L.; Chance, B.; Ching, Y.; Angiolillo, P. *Biophys. J.* **1981**, *34*, 465–498.
(69) Thomson, A. J.; Greenwood, C.; Gadsby, P. M. A.; Peterson, J.; Eglinton, D. G.; Hill, B. C.; Nicholls, P. *J. Inorg. Biochem.* **1985**, *23*, 187–197.
(70) Collman, J. P.; Yang, Y.; Dey, A.; Decreau, R. A.; Ghosh, S.; Ohta, T.; Solomon, E. I. *Proc. Natl. Acad. Sci. U.S.A.* **2008**, *105*, 15660–15665.
(71) Wang, J. L.; Takahashi, S.; Hosler, J. P.; Mitchell, D. M.; Ferguson-Miller, S.; Gennis, R. B.; Rousseau, D. L. *Biochemistry* **1995**, *34*, 9819–9825.
(72) Das, T. K.; Tomson, F. L.; Gennis, R. B.; Gordon, M.; Rousseau, D. L. *Biophys. J.* **2001**, *80*, 2039–2045.

Table 4. Kinetic Parameters of NO Binding to Ferric and Ferrous States of WT Mb and Its Mutants[a]

Mb	k_{on} ($\mu M^{-1}s^{-1}$)	k_{off} (s^{-1})	K_{NO} (μM^{-1})	refs
		$Mb^{III}(NO)$		
WT	0.08	12	0.0067	73, 75
His64Gln	8.2	59	0.19	73, 75
His64Leu	44	80	0.55	73, 75
His64Val	160	120	1.3	73
		$Mb^{II}(NO)$		
WT	22	0.00010	220 000	39, 73, 74
His64Gln	43	0.00011	370 000	39, 74
His64Leu	190	0.00013	1 500 000	39, 74
His64Val	270	0.0011	250 000	73

[a] k_{on} = NO association rate constant, k_{off} = NO dissociation rate constant, K_{NO} = NO affinity constant (k_{on}/k_{off}).

show this effect. Its $Fe^{III}(NO)$ adduct (ν_{FeN}/ν_{NO} = 594/1904 cm^{-1})[7] falls on the imidazole-less line (Figure 13, red line), indicating that the protein site is less constrained than the model.

In addition to NP1, several other proteins occupy intermediate positions in Figure 13; a dashed line has been drawn through them to guide the eye. One of them is the Mb variant H64L/V68N, in which the distal His is absent, but a new potential donor is introduced in place of Val68, at the side of the bound NO (Figure 2). This orientation may limit lone-pair donation by the carbonyl O^{ϵ} atom of the Asn68 side chain, accounting for the intermediate ν_{FeN}/ν_{NO} point. However, Asn68 could also increase positive polarity of the distal environment via its $N^{\epsilon}H$ atoms, thereby enhancing backbonding, as reflected in the elevated ν_{FeN}. Backbonding is even more pronounced for the $Fe^{III}(NO)$ adduct of horseradish peroxidase (HRP), which has unusually high ν_{FeN} (Figure 13), while having an intermediate ν_{NO}. Distal Arg, as well as His, residues enhance positive polarity in HRP. Meanwhile, the distal His (or an intervening water molecule, as judged from the crystal structure of the $Fe^{II}(CO)$ adduct, pdb ID: 1ATJ) can provide lone-pair donation. However, the ν_{NO} value may in this case be limited by the anionic character of the strongly H-bonded proximal His ligand. This effect was also seen in the $Fe^{II}(CO)$ adduct of HRP, for which the ν_{FeC}/ν_{CO} point falls below the neutral His ligand backbonding line.[43]

Energetics of the Lone-Pair Interaction. The switch from H-bond donation by a distal His for $Fe^{II}(NO)$ to lone-pair donation for $Fe^{III}(NO)$ is a natural consequence of the increase in positive charge on the bound NO ligand. The lone-pair interaction stabilizes the $Fe^{III}(NO)$ unit modestly, as can be seen from the changes in the NO association rate (k_{on}), dissociation rate (k_{off}), and association equilibrium (K_{NO}) constants, shown in Table 4. Mutation of His64 to apolar amino acids results in an ~7- to 10-fold increase in the rate constant for NO dissociation, k_{off}, from the $Fe^{III}(NO)$ adduct of Mb (Table 4).[73] Assuming that the slowing of NO dissociation by His64 reflects the lone-pair stabilization energy, the factor of 7−10 translates to stabilization of bound NO in native ferric Mb by −1.0 to −1.3 kcal/mol (i.e., $-RT\ \ln(k_{off,mutant}/k_{off,wt})$).[39] This estimate agrees well with our DFT-computed energy released upon moving a distal imidazole from a nonbonded distance of 3.4 Å to its optimum distance, 2.8 Å, ~−1.2 kcal/mol for the C_s model (which does not induce bending, Figure S3). This interpretation is supported by the results for the His64 to Gln64 mutation in

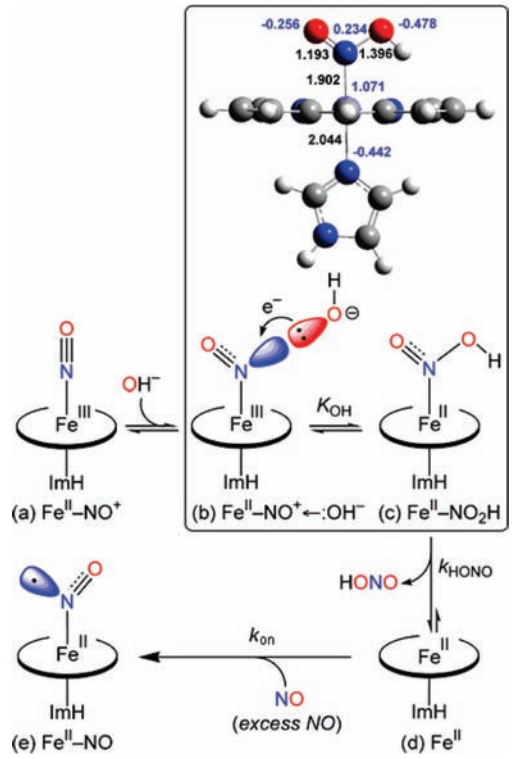

Figure 14. Proposed pathway for reductive nitrosylation of $Fe^{III}(NO)P$. Inset: DFT-optimized structure of the adduct obtained as a result of interaction between HO^- and $(ImH)Fe^{III}(NO)P$. Indicated are bond distances (Å, black) and Mulliken charges (blue).

which lone-pair donation from the O^{ϵ} atom is possible, perhaps accounting for the smaller 5-fold increase in k_{off} for this variant (Table 4).

The NO affinity of $Fe^{III}Mb$ is markedly increased ~30-, 80-, and 200-fold for the Gln64, Leu64, and Val64 variants, respectively, because the NO *association* rate constants, k_{on}, increase ~100- to 2000-fold (Table 4).[73] The slower bimolecular rates for NO binding to native $Fe^{III}Mb$ reflect the free energy barrier for displacement of the water molecule coordinated to the iron atom, which in wild-type $Fe^{III}Mb$ is also stabilized by lone-pair donation by His64. As described by Olson and Phillips,[39] the unfavorable free energy required to disrupt water coordination can be estimated from $RT\ \ln(k_{on,mutant}/k_{on,wt})$ and the value is ~+3 to +4 kcal/mol, which is substantially larger than the favorable $Fe^{III}(NO)$ lone-pair interaction energy that stabilizes NO coordinated to $Fe^{III}Mb$. The net result is that the affinity of wild-type $Fe^{III}Mb$ for NO is very small compared to that for the apolar Val64 or Leu64 $Fe^{III}Mb$ mutants (Table 4). The same His64 mutations also increase the association rate constant for NO binding to $Fe^{II}Mb$, but in this case, the increases in k_{on} for $Fe^{II}Mb$ are much smaller (10- to 20-fold) than those for $Fe^{III}Mb$ (500- to 1000-fold, Table 4). The favorable free energy associated with proton donation by His64 to NO bound to $Fe^{II}Mb$, estimated from the ratio of the mutant versus wt NO dissociation rate constants (≤~1 kcal/mol), is equal to or only slightly smaller than the unfavorable free energy associated with displacement of noncoordinated, internal water H-bonded to the

(73) Foley, E. W. Ph.D. Dissertation, Rice University, Houston, TX, 2006.

(74) Brucker, E. A.; Olson, J. S.; Ikeda-Saito, M.; Phillips, J. G. N. *Proteins: Struct., Funct., Genet.* **1998**, *30*, 352–356.

(75) Eich, R. F.; Li, T.; Lemon, D. D.; Doherty, D. H.; Curry, S. R.; Aitken, J. F.; Mathews, A. J.; Johnson, K. A.; Smith, R. D.; Phillips, G. N.; Olson, J. S. *Biochemistry* **1996**, *35*, 6976–6983.

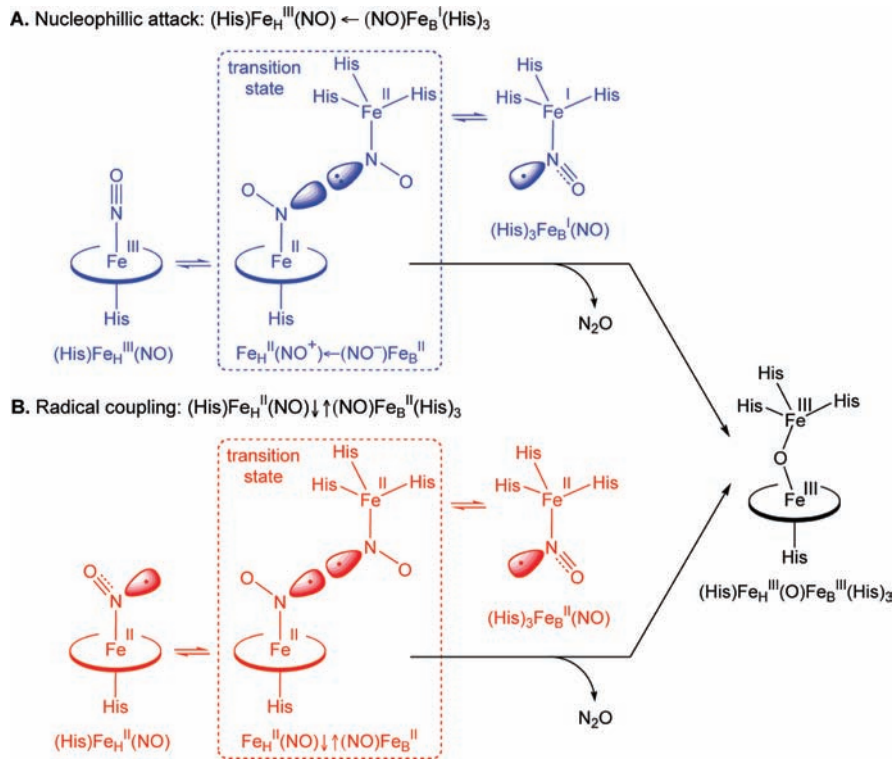

Figure 15. Alternative pathways for N_2O production from the diferrous complex of the NOR binuclear model compund.[70,79]

distal histidine in Fe^{II}Mb, which can be estimated from the ratio of the corresponding association constants (~+1.3 kcal/mol). The net result is that, unlike the situation for Fe^{III}Mb, only small changes in NO affinity for Fe^{II}Mb are observed for His64 mutations (Table 4).[39]

Fe^{III}(NO) Bending by Nucleophilic Attack: Reductive Nitrosylation and NO Reduction. Because electron-withdrawing substituents are absent in protoporphyrin IX, a distal imidazole is attracted mainly to the O_{NO} atom of Fe^{III}(NO) in ferriheme proteins. This is true also of water molecules (see above) or peptide carbonyl groups.[58] However, it is likely that stronger nucleophiles would shift to the N_{NO} atom, bending the Fe^{III}−N−O unit and interacting with the sp^2 orbital.

Nucleophile-induced bending is the likely pathway for "reductive nitrosylation",[76−78] in which hydroxide ion attacks the bound NO, forming nitrous acid, HONO, and Fe(II) heme (Figure 14). The Fe(II) heme is trapped by coordination with excess NO. Consistent with this mechanism, the rate of Fe^{III}(NO) autoreduction increases rapidly with increasing pH.[78] To model this pathway, we carried out DFT optimization of (ImH)Fe^{III}(NO)P with a hydroxide ion placed in proximity to the bound NO. Formation of a HONO intermediate has been proposed, based on kinetic studies of reductive nitrosylation in buffered solutions of Mb^{III}, Hb^{III}, and Cyt^{III}.[76] Consistent with this proposal, the modeled HO$^-$ promptly attacked the N_{NO} atom, causing bending of the Fe^{III}(NO) unit and formation of a stable HONO adduct (Figure 14, inset). This adduct is characterized by elongated Fe−N_{HONO} and Fe−N_{Im^p} bonds and a lowered Mulliken charge on Fe (1.071e vs 1.106e for the starting Fe^{III}(NO) porphine), consistent with Fe reduction. In principle, a similar mechanism of reductive nitrosylation could be available to other nucleophiles, including nitrite, thiols, and amines.

We speculate that NO reduction to N_2O might proceed by a similar pathway, with bound NO$^-$ providing the nucleophile for N−N bond formation. Collman and co-workers have shown that their model compound for the binuclear nitric oxide reductase produces N_2O and an Fe^{III}−O−Fe^{III} adduct upon treatment of the diferrous compound with NO.[70] They were able to detect intermediates with NO bound successively to the non-porphyrin and the porphyrin Fe(II),[79] providing evidence for a "trans" mechanism, in which the reacting NO molecules reside transiently on both Fe atoms of the binuclear complex. The reaction pathway for this di-NO adduct is uncertain but might involve electron transfer from the heme to the non-heme Fe(II), producing Fe$_B^I$(NO) at the non-heme Fe_B site, capable of nucleophilic attack on the heme Fe^{III}(NO) (Figure 15a). The driving force would be stabilization of the Fe(III) by the porphyrinate dianion and of the Fe(I) by the neutral histidine ligands at the non-heme site. The much higher Fe(III/II) reduction potential of the heme than the non-heme site, 0.32 vs 0.06 V,[70] is consistent with this site preference. Alternatively (Figure 15b), the first step in the pathway could be coupling of the two Fe(II)-bound NO neutral radicals, accompanied by concerted electron transfer from the two Fe(II)'s. However, spin restriction and the asymmetry of the binuclear site argue against this symmetric mechanism. The choice between the two pathways will rest upon detailed computation of the energy landscape for electron reorganization. However, the energy landscape may differ somewhat between the model compound and the NOR enzyme, since, as noted above, the model and

(76) Hoshino, M.; Maeda, M.; Konishi, R.; Seki, H.; Ford, P. C. *J. Am. Chem. Soc.* **1996**, *118*, 5702–5707.
(77) Fernandez, B. O.; Lorkovic, I. M.; Ford, P. C. *Inorg. Chem.* **2004**, *43*, 5393–5402.
(78) Ford, P. C.; Fernandez, B. O.; Lim, M. D. *Chem. Rev.* **2005**, *105*, 2439–2455.
(79) Collman, J. P.; Dey, A.; Yang, Y.; Decreau, R. A.; Ohta, T.; Solomon, E. I. *J. Am. Chem. Soc.* **2008**, *130*, 16498–16499.

the protein differ significantly in their $Fe^{III}(NO)$ vibrational frequencies, in a manner suggesting greater rigidity in the model.

$Fe^{III}(NO)$ Bending by Thiolate Ligation: Cysteinyl Hemes. In addition to a lone-pair interaction at the N_{NO} atom, $Fe^{III}-N-O$ bending can be induced by mixing of the d_{z^2} and d_{xz} orbitals, or more precisely the d_{z^2}-σ_n and d_{xz}-π^*_{NO} orbitals, as has been discussed by others.[80−83] This is the source of bending when thiolate is a ligand. The strongly donating RS^- drives up the d_{z^2}-σ_n energy, and increases its mixing with d_{xz}-π^*_{NO}. The crystal structure of a thiolate-ligated $Fe^{III}(NO)$ adduct reveals a 160° Fe−N−O angle,[84] consistent with structures of cysteinyl heme proteins,[28,29,85] which also produce a positive ν_{FeN}/ν_{NO} correlation (Figure 1). For the model complex $(CH_3S^-)Fe^{III}(NO)P$, Linder and Rodgers computed an Fe−N−O angle of 159°, which increased to 180° when the CH_3S^- was protonated, thereby lowering its donor strength.[58] Paulat and Lehnert computed structures and vibrational frequencies for $Fe^{III}(NO)P$, with thiolate ligands having zero, one and two H-bonds to the sulfur atom.[86] Both ν_{FeN} and ν_{NO} increased as the number of H-bonds increased, reflecting diminished d_{z^2}-σ_n/d_{xz}-π^*_{NO} mixing as the thiolate donor strength diminished. A similar effect underlies the cysteinyl heme protein ν_{FeN}/ν_{NO} correlation in Figure 1. The ν_{FeN}/ν_{NO} frequencies increase in the order cytochrome $P450_{cam}$ < cytochrome $P450_{nor}$ < chloroperoxidase (CPO), which is also the order of increased H-bonding to the cysteinyl sulfur, as judged by analyses of the crystal structures[5] and also by vibrational data on the corresponding CO adducts.[43]

Conclusions

For imidazole-ligated $Fe^{III}(NO)$ adducts ν_{FeN} and ν_{NO} are negatively correlated, consistent with variations in backbonding, but distal lone-pair donors induce an additional increase in ν_{NO} due to a specific orbital interaction. These donors can include imidazole, but also peptide carbonyl groups and water molecules. The lone-pair interaction of a distal imidazole represents approximately −1.0 to −1.3 kcal/mol of stabilization energy.

The ν_{FeN} and ν_{NO} frequencies become positively correlated when the $Fe^{III}(NO)$ moiety bends, since the $Fe^{III}-NO$ and N−O bonds are then weakened simultaneously. Bending can be induced by different stereoelectronic mechanisms, including the following:

1. electron-donating substituents at the heme *meso*-positions, which induce mixing of the porphyrin a_{2u}-type orbital with a bending-induced antibonding combination of d_{xz} and π^*_{NO} orbitals;

2. a distal lone pair drawn close enough by electron-withdrawing β-substituents, or by strong nucleophilicity, to interact with a bending-induced sp^2-like orbital on N_{NO}; and

3. a strongly donating proximal axial ligand that raises the d_{z^2} orbital energy and induces mixing of the d_{z^2}-σ_n and d_{xz}-π^*_{NO} orbitals.

The first two of these mechanisms are generally inapplicable to heme proteins, since the protoporphyrin IX *meso*-substituents (−H) are not electron-donating and the β-substituents (methyl, vinyl, propionate) are not electron-withdrawing, and since the available lone-pair donors are generally weak nucleophiles. However, attack of a strong nucleophile is facilitated by bending-induced exposure of the empty orbital on the N_{NO} atom. Examples include attack of hydroxide to form a transient HONO adduct, during reductive nitrosylation, and possibly the attack of Fe_B-bound NO^- in the NO coupling reaction induced by NO reductase.

The third mechanism is operative in heme proteins with the strongly donating cysteinate ligand. Here, the ν_{FeN} and ν_{NO} frequencies are positively correlated, with the degree of bending modulated by H-bond donation to the cysteinate.

Acknowledgment. This work was supported financially by NIH Grants GM033576 (T.G.S.), GM035649 (J.S.O.), and HL047020 (J.S.O.) and by Robert A. Welch Foundation Grants C-0612 (J.S.O.) and E-1184 (R.S.C.).

Supporting Information Available: Complete ref 34 RR difference spectra (^{14}NO − ^{15}NO) for $Fe^{III}(NO)$ adducts of Mb variants having distal His64 replaced by Gln (Figure S1), distal $ImH\cdots N_{NO}$ distance dependence for the $(ImH)Fe^{III}(NO)\cdots(ImH)$ porphine complex in C_1 symmetry (Table S1, Figure S2), distal $ImH\cdots O_{NO}$ distance dependence for the $(ImH)Fe^{III}(NO)\cdots(ImH)$ porphine complex in C_s symmetry (Table S2, Figure S3), and Cartesian coordinates of DFT-optimized structures for the models depicted in Figure 9 (Table S3). This material is available free of charge via the Internet at http://pubs.acs.org.

JA906233M

(80) Mingos, D. M. P. *Inorg. Chem.* **1973**, *12*, 1209–1211.
(81) Pierpont, C. G.; Eisenberg, R. *J. Am. Chem. Soc.* **1971**, *93*, 4905–4907.
(82) Hawkins, T. W.; Hall, M. B. *Inorg. Chem.* **1980**, *19*, 1735–1739.
(83) Hoffmann, R.; Chen, M. M.-L.; Thorn, D. L. *Inorg. Chem.* **1976**, *16*, 503–511.
(84) Xu, N.; Powell, D. R.; Cheng, L.; Richter-Addo, G. B. *Chem. Commun.* **2006**, 2030–2032.
(85) Pant, K.; Crane, B. R. *Biochemistry* **2006**, *45*, 2537–2544.
(86) Paulat, F.; Lehnert, N. *Inorg. Chem.* **2007**, *46*, 1547–1549.